Biosensors and Bioelectronics 26 (2011) 2987–2993

Contents lists available at ScienceDirect

Biosensors and Bioelectronics

journal homepage: www.elsevier.com/locate/bios

Nanocrystalline diamond impedimetric aptasensor for the label-free detection of human IgE

Dinh T. Tran[a], Veronique Vermeeren[b], Lars Grieten[c], Sylvia Wenmackers[c], Patrick Wagner[c,d], Jeroen Pollet[a], Kris P.F. Janssen[a], Luc Michiels[b], Jeroen Lammertyn[a,*]

[a] BIOSYST-MeBioS, Katholieke Universiteit Leuven, Willem de Croylaan 42, B-3001 Leuven, Belgium
[b] Biomedical Research Institute, School for Life Sciences, Hasselt University and Transnationale Universiteit Limburg, Agoralaan, Building C, B-3590 Diepenbeek, Belgium
[c] Institute for Materials Research, School for Life Sciences, Hasselt University and Transnationale Universiteit Limburg, Wetenschapspark 1, B-3590 Diepenbeek, Belgium
[d] IMEC, Division IMOMEC, Wetenschapspark 1, B-3590 Diepenbeek, Belgium

ARTICLE INFO

Article history:
Received 17 September 2010
Received in revised form
19 November 2010
Accepted 30 November 2010
Available online 5 December 2010

Keywords:
Aptamer
Biosensor
Human IgE
Electrochemical impedance spectroscopy
Nanocrystalline diamond

ABSTRACT

Like antibodies, aptamers are highly valuable as bioreceptor molecules for protein biomarkers because of their excellent selectivity, specificity and stability. The integration of aptamers with semiconducting materials offers great potential for the development of reliable aptasensors. In this paper we present an aptamer-based impedimetric biosensor using a nanocrystalline diamond (NCD) film as a working electrode for the direct and label-free detection of human immunoglobulin E (IgE).

Amino (NH_2)-terminated IgE aptamers were covalently attached to carboxyl (COOH)-modified NCD surfaces using carbodiimide chemistry. Electrochemical impedance spectroscopy (EIS) was applied to measure the changes in interfacial electrical properties that arise when the aptamer-functionalized diamond surface was exposed to IgE solutions. During incubation, the formation of aptamer–IgE complexes caused a significant change in the capacitance of the double-layer, in good correspondence with the IgE concentration. The linear dynamic range of IgE detection was from 0.03 μg/mL to 42.8 μg/mL. The detection limit of the aptasensor reached physiologically relevant concentrations (0.03 μg/mL). The NCD-based aptasensor was demonstrated to be highly selective even in the presence of a large excess of IgG. In addition, the aptasensor provided reproducible signals during six regeneration cycles. The impedimetric aptasensor was successfully tested on human serum samples, which opens up the potential of using EIS for direct and label-free detection of IgE levels in blood serum.

1. Introduction

Allergenicity is a major health concern in both children and adults. Approximately 2% of adults and 8% of children suffer from allergenicity (Sampson, 1999). Allergic reactions are caused by exposure of the skin to chemicals, or of the respiratory system to pollen or dust, and consumption of certain food products (Kim et al., 2009). Human immunoglobulin E (IgE) has been demonstrated to be a mediator in diseases of immediate type hypersensitivity. Therefore, the total IgE level in serum is widely reported as a marker of atopic diseases (Buravkova et al., 2007; Jackola et al., 2004). An adult is considered to be atopic when the total IgE serum level lies above 100 IU/mL (Wuthrich et al., 1996).

Currently, enzyme-linked immunosorbent assay (ELISA) technology using antibodies for quantification of serum IgE is commercially available (Diagnostics Automation, INC, CA, USA). Next to traditional immunoassay methods, several aptamer-based techniques have been developed to detect IgE including capillary electrophoresis (CE) (German et al., 1998), fluorescence anisotropy (Gokulrangan et al., 2005), surface plasmon resonance (SPR) (Pollet et al., 2009), and quartz crystal microbalance (QCM) (Yao et al., 2009). In contrast with these sensing platforms, electrochemical impedance spectroscopy (EIS)-based molecular detection offers the advantage that it is not only sensitive and selective but also well suited for integration in a very compact and portable biosensor. It has been proven that EIS can be successfully used as an immunosensor (Berggren et al., 2001; Cooreman et al., 2005), an enzyme sensor

* Corresponding author. Tel.: +32 16 321459; fax: +32 16 321614.
E-mail addresses: thidinh.tran@biw.kuleuven.be (D.T. Tran), veronique.vermeeren@uhasselt.be (V. Vermeeren), lars.grieten@uhasselt.be (L. Grieten), sylvia.wenmackers@uhasselt.be (S. Wenmackers), patrick.wagner@uhasselt.be (P. Wagner), jeroen.pollet@biw.kuleuven.be (J. Pollet), kris.janssen@biw.kuleuven.be (K.P.F. Janssen), luc.michiels@uhasselt.be (L. Michiels), jeroen.lammertyn@biw.kuleuven.be (J. Lammertyn).

0956-5663/$ – see front matter © 2010 Elsevier B.V. All rights reserved.
doi:10.1016/j.bios.2010.11.053

(Alfonta et al., 2001; Kharitonov et al., 2000), and a DNA sensor (Cai et al., 2003; Lee and Shim, 2001; Vermeeren et al., 2007; Yang et al., 2004).

Synthetic diamond has been studied extensively as a transducer material for biosensor fabrication because of its very appealing physical, chemical, and electrical characteristics (Swain and Ramesham, 1993). It has a wide electrochemical potential window, is chemically inert, and can be made electrically semiconductive by chemical doping (Koizumi et al., 1997; Nebel et al., 2007; Williams and Nesladek, 2006). In addition, various procedures have been developed to covalently attach biomolecules to diamond, such as chemical (Ushizawa et al., 2002), photochemical (Härtl et al., 2004; Vermeeren et al., 2008; Wenmackers et al., 2009; Yang et al., 2002), and electrochemical methods (Uetsuka et al., 2007). These linkages were demonstrated to be more stable than those with other commonly used electrode materials, such as gold (Au), Si, glass and glassy carbon (Yang et al., 2002). Moreover, diamond is biocompatible (Smisdom et al., 2009; Tang et al., 1995), therefore allowing *in vivo* electronic applications.

In this paper, we describe the development of a novel nanocrystalline diamond (NCD)-based aptasensor for the label-free detection of human IgE using EIS. We investigated the influence of IgE binding to the aptamer receptor on the impedance properties of the system. Furthermore, we showed that changes in capacitance of the double-layer relate directly to the concentration of the desired analyte. Our findings demonstrate the potential of using NCD-based EIS in combination with aptamers to directly measure IgE levels.

2. Materials and methods

2.1. Materials

The anti-IgE aptamer originally selected by Wiegand et al. (1996) was synthesized by Eurogentec (Luik, Belgium). The aptamer was extended with 20 thymidine bases at the 5′ amino (NH_2)-binding site to give the aptamer its maximum flexibility for binding with IgE proteins. For characterization of the NCD surface, the aptamer was also labeled at the 3′ end with an Alexa Fluor® 488 label. The full sequence of the aptamer is 5′-NH_2-C_6H_{12}-TTTTTTTTTTTTTTTTTTTTGGGGCACGTTTATCCGTCCCTCCTAGTGGCG TGCCCC-3′. IgE from human myeloma plasma, with an isoelectric point (pI) of 9, was supplied by Athens Research and Technology (Georgia, USA). Human IgG and 10-undecenoic acid were supplied by Sigma–Aldrich (Bornem, Belgium). Bovine serum albumin (BSA) was purchased from Roche Diagnostics (Vilvoorde, Belgium), 1-ethyl-3-(3-dimethylaminopropyl)-carbodiimide (EDC) and 2-[N-morpholino]-ethanesulphonic acid (MES) were purchased from Perbio Science (Erembodegem, Belgium). Trizma base, potassium phosphate dibasic (K_2HPO_4), glycine, sodium chloride (NaCl), and sodium hydroxide (NaOH) were purchased from ACROS (New Jersey, USA).

The buffer used for electrochemical impedance measurements consisted of 25 mM trizma base, 192 mM glycine, and 5 mM K_2HPO_4 (TGK) at a pH of 8.3.

2.2. NCD sensor fabrication

Commercially available H-terminated NCD wafers, grown by hot filament chemical vapour deposition (HFCVD) from rho-BeSt (Innsbruck, Austria), were used. The wafers consisted of a 2–4 μm thick NCD film with a grain size of 5–15 nm, grown on p-type silicon. Further treatment of the wafers can be found in Vermeeren et al. (2008). Briefly, the wafers were cut into 1 cm^2 pieces using a diamond scribe and cleaned for 30 min in an oxidizing mixture containing 100 mL of H_2SO_4 18 M and 50 mg KNO_3 at 100 °C for 2 h. This procedure was followed by washing in an ultrasonic bath with distilled, ultrapure water at room temperature. Afterwards, the samples were thoroughly rinsed with heated distilled, ultrapure water and dried with nitrogen gas. Before use, the samples were hydrogenated at 700 °C for 60 s at 3000 W, 35 Torr, and 1000 sccm H_2.

2.3. NCD sensor functionalization

Three NCD surfaces were incubated with a 50 μL droplet of the mixture containing different amounts of NH_2 modified and Alexa 488-labeled aptamer (5 pmol, 50 pmol and 500 pmol) and 5 μmol of EDC in a 25 mM MES buffer (pH 6) according to the protocol described by Vermeeren et al. (2008). In brief, unsaturated fatty acid (10-UDA) was first photochemically attached to the H-terminated NCD. In the second step, NH_2-terminated IgE aptamers were covalently linked to COOH-modified NCD surface using EDC coupling. As a negative control, one surface was treated with the mixture containing 500 pmol aptamer but EDC was replaced by an equal volume of MES buffer. Finally, the aptamer-coated NCD electrodes were immersed in 1 × PBS buffer with 6% BSA at 4 °C overnight to reduce non-specific binding of IgE onto the NCD surface.

The fluorescence intensity of the aptamer-functionalized NCD surfaces was measured using a Zeiss LSM 510 META Axioskop 2 FS Mot laser scanning confocal fluorescence microscope. The NCD samples were excited with 10% laser intensity of the 488 nm line of an argon-ion laser. The fluorescence emission was selected with a long pass filter BP 500–550, using beam splitters HFT UV/488/543/633.

All images were collected with a W Plan-Apochromat 10 × NA 0.3 W Ph1. The image size was 1024 × 1024 pixels. The pinhole size was 1.97 airy unit. Pixel dwell time was 1.60 μs. The detector gain was set at 1000.

2.4. Sensor setup

The sensor setup used in our study is represented in Fig. 1A, similar to that used by Bijnens et al. (2009). Four separate NCD samples of 1 cm^2 coated with anti-IgE aptamer, functioning as working electrodes were mounted onto a Cu plate back contact using Ag paste. Rubber O-rings with an inner-diameter of 7 mm and a Teflon lid containing 4 circular holes of equal size were pressed onto the samples to create 4 reaction wells above the NCD.

The wells were filled with 140 μL of reaction fluid. Four gold wires, one for each reaction well, placed ∼1 mm above the NCD surface in contact with the reaction fluid, were used as counter electrodes. The working and counter electrodes were connected to the impedance analyzer with shielded cables. This set-up allows the recording of 4 signals simultaneously.

2.5. Impedance spectroscopy

Impedance spectroscopy was performed using a Hewlett Packard 4248 A precision LCR meter (Agilent, Diegem, Belgium). The impedance was measured by applying a small, sinusoidally modulated voltage (U) of 10 mV to the measurement cell. The response to this potential is an AC signal (I). The complex impedance (Z) was measured for 25 frequencies in a frequency range from 20 Hz to 100 kHz. The duration of one frequency sweep was 2.35 min.

Real-time impedance spectra were collected continuously during stabilization, analyte addition and rinsing. The reaction wells were first filled with 130 μL TGK buffer, and the device was allowed to stabilize until no further change in Z between two successive frequency sweeps was detected throughout the entire frequency range. Then, 10 μL of samples containing target protein (IgE or

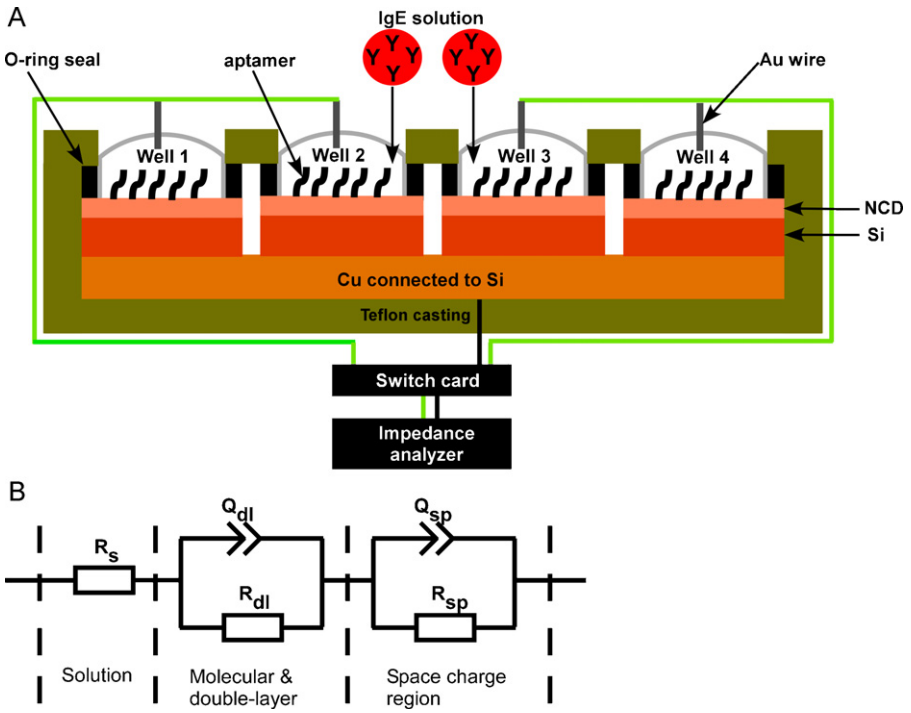

Fig. 1. (A) Schematic illustration of the aptasensor setup with four reaction wells. (B) The electrical circuit model describing the chemically modified electrode system used to fit the experimental data.

IgG) was injected into the buffer in each well. The mixture was left to incubate for 1 h. Subsequently, the wells were rinsed and refilled with buffer, and the signal was allowed to stabilize for at least 45 min prior to denaturation of the aptamers for reuse. The IgE–aptamer complex was denatured by filling the wells with 100 μL of denaturation buffer containing 0.05 M NaOH and 1 M NaCl for 10 min. This step was repeated twice. Finally, the device was again stabilized with fresh buffer and used for the next cycles.

For all impedance experiments, the sensor setup was placed in a humidity-controlled hybridization oven at 37 °C, which also resulted in electromagnetic shielding.

2.6. Analysis of impedance data

The electrical circuit parameters were determined by fitting the impedance data to the equivalent circuit given in Fig. 1B. The fits were performed over the total frequency range from 20 Hz to 100 kHz using the non-linear least-squares fit principles performed with ZSimpWin software from Princeton Applied Research (Massachusetts, USA). The circuit consists of three components connected in series: the solution resistance R_s, between the gold electrode and the NCD surface, a resistance R_{dl} and a constant phase element (CPE) Q_{dl} in parallel, corresponding to the molecular layer and its associated double-layer on the NCD surface, and a resistance R_{sp} and a CPE Q_{dl} in parallel, corresponding to the space-charge region in the NCD.

2.7. Clinical sample analysis

To illustrate the feasibility of using the presented aptasensor to measure IgE concentrations in biological samples, different IgE concentrations were added to a sample of commercially available human serum (Sigma–Aldrich, Bornem, Belgium). After stabilizing the sensor with TGK buffer, IgE spiked serum was injected into the well to obtain final concentrations of 0.05 μg/mL, 0.4 μg/mL, 1.5 μg/mL, 2.9 μg/mL, 5.8 μg/mL, 11.7 μg/mL, 23.3 μg/mL, and 46.7 μg/mL. The measurement protocol for the serum samples was the same as that of IgE in buffer described in Section 2.5.

To validate the aptasensor results, a commercially available ELISA kit (Diagnostics Automation, INC, CA, USA) for IgE determination was used as a benchmark to analyze all these serum samples. When necessary, serum samples that had concentration levels outside of the measurement range of the ELISA kit were diluted for measurement. The ELISA assay was performed according to the instructions of the manufacturer.

3. Results and discussion

3.1. Functionalization of the NCD surface with aptamers

To make sure that the NCD samples could effectively be functionalized with aptamer biorecognition molecules, three NCD samples were modified with different amounts of NH_2-modified Alexa 488-labeled aptamer (5 pmol, 50 pmol, and 500 pmol) using an EDC coupling. Another sample, as a negative control, was also treated with 500 pmol aptamer but without EDC. The results of the fluorescent imaging demonstrated that the maximum intensity was obtained for the sample treated with EDC and 500 pmol aptamer (Fig. 2C), which corresponds to 3×10^{14} molecules immobilized on the surface while the negative control showed no fluorescence (Fig. 2D). In the further experiments the NCD surfaces were modified with 500 pmol aptamer.

3.2. Impedance measurement of IgE–aptamer binding

For the detection of IgE in solution, impedance spectroscopy was used to extract electrical properties of the electrolyte/diamond interface. Fig. 3 shows Bode (A) and Nyquist (B) plots obtained before adding 42.8 μg/mL IgE and after 1 h of reaction in a typical experiment. It is noted that 'before adding IgE' can be regarded as an internal reference point, corresponding to a condition where the NCD sensor is completely stabilized with buffer, before addition of

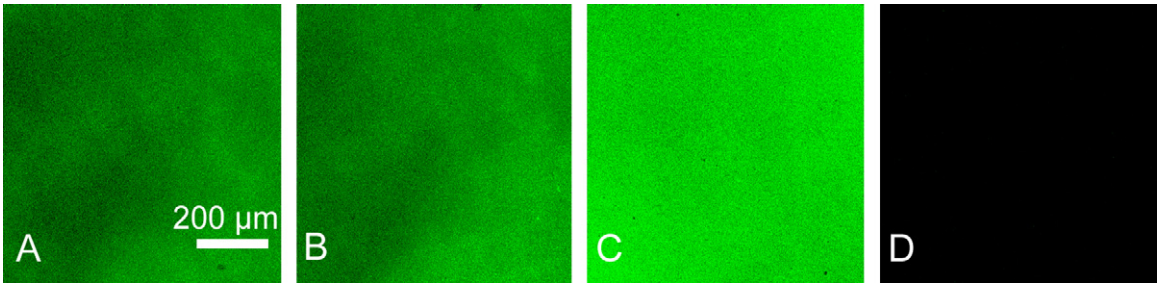

Fig. 2. Fluorescent intensity of the NCD surfaces treated with different amounts of NH_2-modified Alexa 488-labeled aptamer. (A) 5 pmol aptamer with EDC. (B) 50 pmol with EDC. (C) 500 pmol with EDC. (D) 500 pmol without EDC.

analyte, and before any aptamer–IgE complexes are formed. This is done so for every measurement. Exposing the aptamer-coated NCD surfaces to IgE results in a decrease of the complex impedance as shown in the Bode plot. This change is more pronounced at low frequencies (from 20 Hz to 100 Hz) while at high and intermediate frequencies, between 100 Hz and 100 kHz, the two traces are nearly overlapping. This is because in the low frequency range the impedance is dominated by the events in the molecular layer while at high frequencies the impedance is more sensitive to the composition of the buffer solution than the surface capacitance effects (Lasseter et al., 2004) (Fig. 1B).

While the logarithmic impedance plot (Fig. 3A) shows the change in the response over the entire frequency range, the linear Nyquist plot (Fig. 3B) presents more clearly the impedance changes of different layers of the sensor surface. The fits of these data to the given electrical circuit (Fig. 1B) are indicated by solid lines. As can be seen in Fig. 3B, there is an increase of the second semi-circle corresponding to the decrease of the impedance during IgE recognition at low frequency as the result of the formation of the aptamer–IgE conjugated layer on the electrode surface. However, the shape of the high-frequency semi-circle corresponding to the diamond layer remained the same upon exposure to IgE solution. This phenomenon can be due to the fact that at the working buffer pH of 8.3, IgE molecule is slightly positive since its isoelectric point is about 9.0 (Iijima et al., 1999). Therefore, the binding of IgE to the surface could not attribute to the depletion zone in the diamond substrate. This finding is different from the results obtained by Vermeeren et al. (2007) and Yang et al. (2004) on DNA sensors in that their studies observed a clear decrease of impedance at high frequency during hybridization which was not the case in the current study and their observations could be explained by the field-effect mechanism.

3.3. Aptasensor sensitivity and linear dynamic range

To investigate the dynamic range of the impedimetric aptasensor using impedance spectroscopy, different IgE concentrations were added to the TGK buffer in each well so that the final concentrations were 0.2 µg/mL, 0.54 µg/mL, 2.14 µg/mL, 10.7 µg/mL, 21.4 µg/mL, and 42.8 µg/mL. In order to understand the physical meaning of the impedance changes at low frequencies, the circuit shown in Fig. 1B was used to fit the experimental data. The fitting result before and after 1 h of exposure to different concentrations of IgE is given in Table 1. The electrolyte ohmic resistance R_s which is dependent on the ionic strength of the buffer dominates at the highest frequency (100 kHz) thus it is not much affected by the binding reaction of IgE to the surface. The values of R_{sp}, Q_{sp} and n_{sp} do not significantly change after IgE incubation. This means that the formation of IgE–aptamer complexes on the electrode surface does not affect the impedance of the space charge region. However, these complexes contributed to a change of the capacitance value (Q_{dl}) of the molecular layer and its associated double-layer on the surface. This can be well explained by the fact that the additional layer of IgE captured on top of the anti-IgE aptamer layer decreases the dielectric constant of the medium due to the strong solvatation effect of the electric charge and increases the thickness of the biomolecular membrane as well. Both factors lead to a decrease of the capacitance of the electrode surface (Bijnens et al., 2009; Wei et al., 2003). The changes of R_{dl} were not employed because the model fit sometimes gave high uncertainties of this parameter.

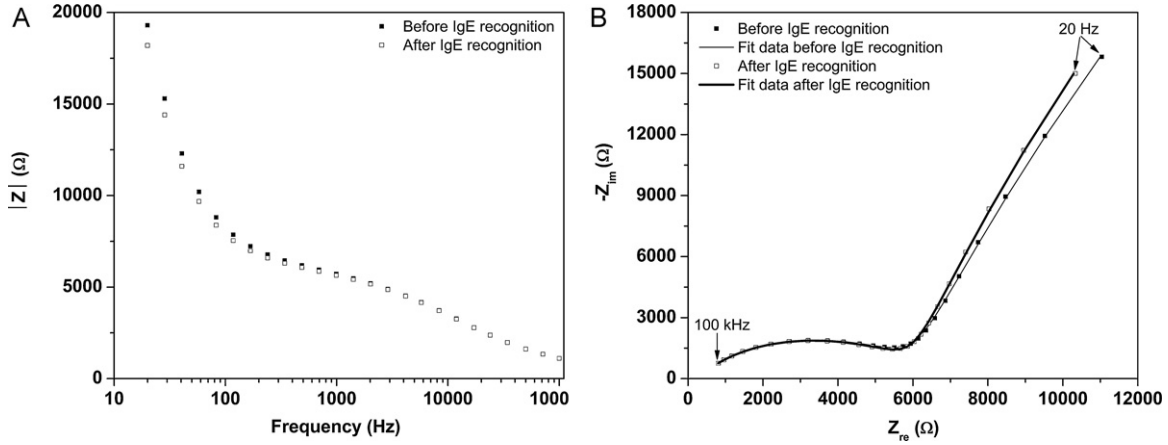

Fig. 3. Impedance measurement of the IgE–aptamer binding. The aptamer-functionalized NCD (500 pmol aptamer) was incubated with 42.8 µg/mL IgE. (A) Bode plot showing the impedance modulus *versus* frequency and (B) Nyquist plot showing the response of the real and the imaginary part of the complex impedance in the total frequency range measured before (■) and after 1 h (□) exposure to IgE. Symbols represent the measured data and solid lines represent the fit curves, based on the equivalent circuit model shown in Fig. 1B.

Table 1
Values of circuit elements obtained by fitting the experimental data from Fig. 3 to the circuit model shown in Fig. 1B.

Circuit element	IgE concentration											
	42.8 μg/mL		21.4 μg/mL		10.7 μg/mL		2.14 μg/mL		0.54 μg/mL		0.2 μg/mL	
	Buffer	Sample	Buffer	Sample	Buffer	Sample	Buffer	Sample	Buffer	Sample	Buffer	Sample
R_s (kΩ)	0.30 ± 0.02[a]	0.29 ± 0.02	0.29 ± 0.02	0.29 ± 0.02	0.37 ± 0.02	0.24 ± 0.02	0.26 ± 0.05	0.24 ± 0.05	0.36 ± 0.02	0.22 ± 0.02	0.43 ± 0.04[a]	0.41 ± 0.04
R_{dl} (kΩ)	251.6 ± 1.2	230.7 ± 1.0	242.1 ± 1.2	213 ± 1.6	Und.	Und.	Und.	Und.	Und.	Und.	Und.	Und.
Q_{dl} (nS s^n)	998.6 ± 1.0	979.1 ± 0.9	984.9 ± 1.1	975.2 ± 1.5	1016 ± 2	1010 ± 2	112.8 ± 0.9	109.8 ± 0.9	1336.0 ± 0.8	1334.0 ± 0.8	470.8 ± 2.3	469. 7 ± 2.3
n_{dl}	0.84 ± 0.01	0.86 ± 0.01	0.85 ± 0.01	0.86 ± 0.02	0.93 ± 0.02	0.92 ± 0.02	1.00 ± 0.04	1.00 ± 0.04	0.86 ± 0.03	0.86 ± 0.03	0.99 ± 0.05	0.99 ± 0.05
R_{sp} (kΩ)	5.74 ± 0.04	5.70 ± 0.03	5.74 ± 0.04	5.73 ± 0.05	4.06 ± 0.05	3.98 ± 0.05	29.4 ± 0.2	29.1 ± 0.2	3.64 ± 0.06	3.58 ± 0.05	24.8 ± 0.1	24.7 ± 0.1
Q_{sp} (nS s^n)	77.1 ± 0.3	74.8 ± 0.3	78.1 ± 0.3	76.9 ± 0.5	45.4 ± 0.4	40.9 ± 0.4	51.7 ± 0.5	51.2 ± 0.5	62.5 ± 0.5	61.3 ± 0.5	28.3 ± 0.3	28.2 ± 0.3
n_{sp}	0.71 ± 0.01	0.71 ± 0.01	0.71 ± 0.01	0.71 ± 0.02	0.85 ± 0.02	0.87 ± 0.05	0.71 ± 0.02	0.71 ± 0.02	0.80 ± 0.02	0.83 ± 0.02	0.75 ± 0.02	0.75 ± 0.02
χ^2	2.2×10^{-5}	1.6×10^{-5}	2.8×10^{-5}	1.3×10^{-4}	4.8×10^{-4}	4.7×10^{-4}	1.2×10^{-3}	1.5×10^{-3}	6.1×10^{-4}	5.7×10^{-4}	5.6×10^{-4}	5.8×10^{-4}

'Buffer': reference signal before adding IgE, 'sample': signal recorded 1 h after adding IgE. The aptasensor showed an excellent linear correlation between the ΔQ_{dl} values and the IgE concentrations.
[a] Reported uncertainties are standard errors as obtained from the data fits. R_{dl} was undefined for the lower IgE concentrations (und.). This can be explained by the fact that R_{dl} is the value of the real part of the impedance, extrapolated from the very low frequency end of another semi-circle in the Nyquist plot.

This can be explained due to the fact that R_{dl} is the value of the real impedance, extrapolated from the second semi-circle in the Nyquist plot. As can be observed in Fig. 3B, only the start of this semi-circle is visible, therefore a high uncertainty was obtained for R_{dl}.

Consequently we used the change of the double-layer capacitance (ΔQ_{dl}) for quantification purposes. Fig. 4A reveals the calibration plot of the IgE detection. The aptasensor showed an excellent linear correlation between the ΔQ_{dl} values and the IgE concentrations, which is desirable for the quantification. The linear relation gave a regression equation of $\Delta Q_{dl} = 0.42[IgE] + 0.535$ with a determination coefficient of 0.994. The limit of detection (LOD) (S/N = 3) was evaluated to be 0.03 μg/mL based on 3 times the standard deviation of the blank (buffer solution in which IgE was diluted). The sensitivity was 0.42 nS s^n mL/μg as calculated from the slope of the calibration curve and the linear dynamic range is as low as 0.03 μg/mL to at least 42.8 μg/mL. There have been a number of studies from different groups using EIS based aptasensors for detection of IgE. For instance, Xu et al. (2005) used aptamer-based array electrodes in which aptamers were immobilized on gold electrodes to detect IgE with a LOD of 0.02 μg/mL, similar to that of our system. Recently, Kara et al. (2010) reported a bioelectronic detection of aptamer–IgE binding based on the EIS technique using disposable graphite working electrodes. A LOD of 0.1 μg/mL was obtained in this case. Although the electrode materials used by these groups are compatible with micro-electronic processes, they are not as chemically stable as diamond and the bio-interfaces may degrade upon contact with aqueous electrolytes (Nebel et al., 2007). Moreover, a redox probe labeling was added to their systems to facilitate the electron transfer resistance, which is not necessary in the current study, making our protocol faster and simpler. Other techniques than EIS have been developed for IgE detection. Gokulrangan et al. (2005) used fluorescence anisotropy technique with LOD of 0.07 μg/mL, which is the same range as that of our aptasensor. However, this technique requires relatively complicated optics. With the commercial ELISA kit for quantification of IgE, the detection limit is 0.01 μg/mL.

3.4. Specificity of the aptasensor

To verify the specificity of the aptasensor, IgG which has an analogous structure to IgE and appears in high concentration in blood sera was used. The specificity was evaluated by comparing ΔQ_{dl} resulting from IgE binding to that from IgG binding to the NCD surface. Fig. 4B shows the Nyquist plot of a typical result obtained before and after 1 h of IgG addition. The impedance modulus after incubating with 32.1 μg/mL IgG almost falls back onto that before recognition. Fig. 4A shows the changes in double-layer capacitance as a function of the protein concentration. As mentioned above, the capacitance changes (ΔQ_{dl}) are proportional to the IgE concentrations in the range from 0.03 μg/mL to 42.8 μg/mL. However, the capacitance changes are negligible for IgG. This result suggests that the aptasensor has very high selectivity towards IgE and exhibits minimal non-specific binding due to successful application of BSA when preparing the electrodes.

3.5. Reusability of the aptasensor

To assess the reusability of our aptasensor, the aptamer-coated NCD electrode that had been incubated with IgE solution in the previous cycle was first rinsed and stabilized with TGK buffer. Then the IgE–aptamer complex was denatured by filling the wells with 100 μL of the denaturation buffer for 10 min. Subsequently, the regenerated sensor was challenged to a next cycle of IgE recogni-

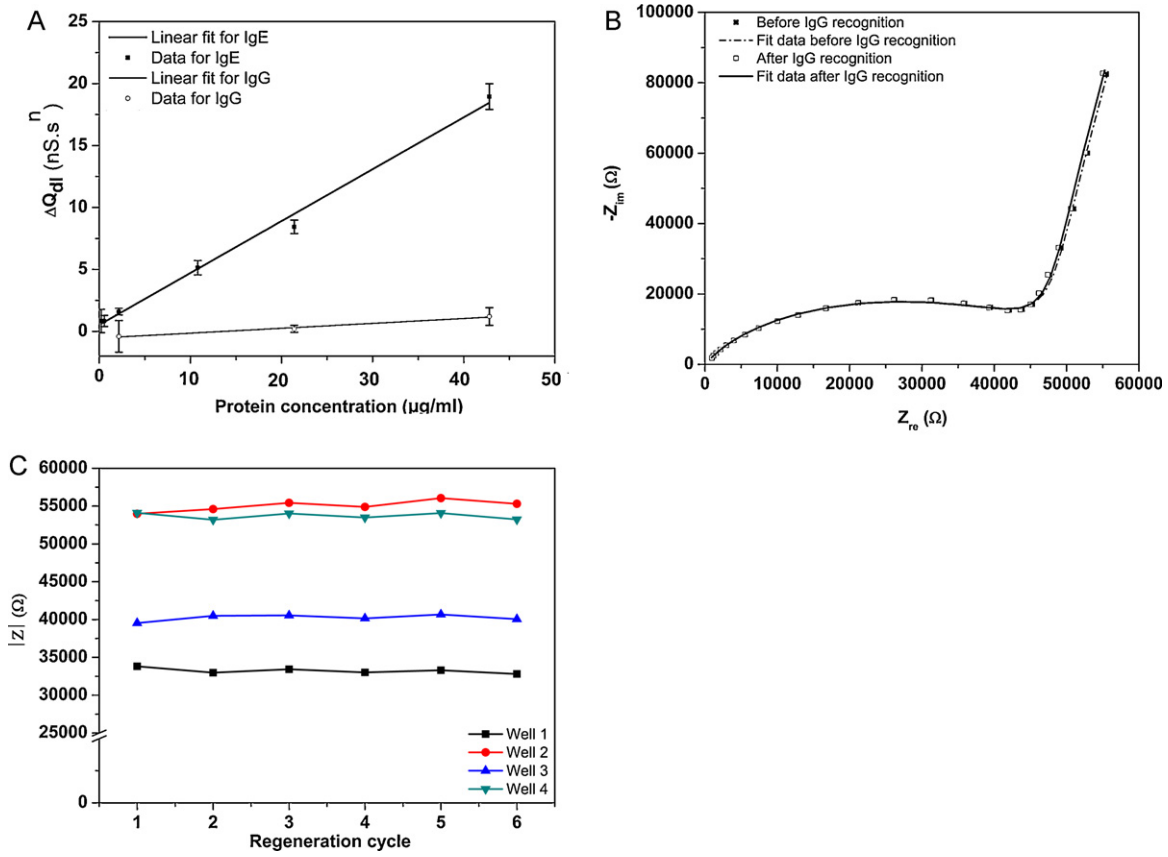

Fig. 4. (A) Dose–response curve of the aptasensor to IgE (■) and IgG (○) at different concentrations (0.2–42.8 μg/mL). Each point represents the average of three measurements. Error bars present standard errors. (B) Nyquist plot of the aptamer-coated NCD sensor obtained before (■) and 1 h after adding 32.1 μg/mL of IgG (□). (C) The reusability of the aptasensor during six repeated cycles.

tion and the impedance spectra were recorded again. Fig. 4C shows the complex impedance values (Z) at 82 Hz of the regenerated surface during six repeated cycles for four reaction wells. The relative standard deviations (R.S.D.) of the complex impedance at 82 Hz for six regeneration cycles were found to be 1.1%, 1.3%, 1% and 0.8% for well 1, well 2, well 3 and well 4, respectively. This result indicates that the aptasensor was reusable; the aptamer probe layer is not damaged by the denaturation steps. This is due to the covalent attachment approach for the immobilization leading to a very stable aptamer-diamond interface.

3.6. Application of the aptasensor in biological samples

The practical application of the aptasensor was demonstrated by measuring IgE levels in human serum samples. Fig. 5A shows the dose–response curve of IgE detection using the aptasensor.

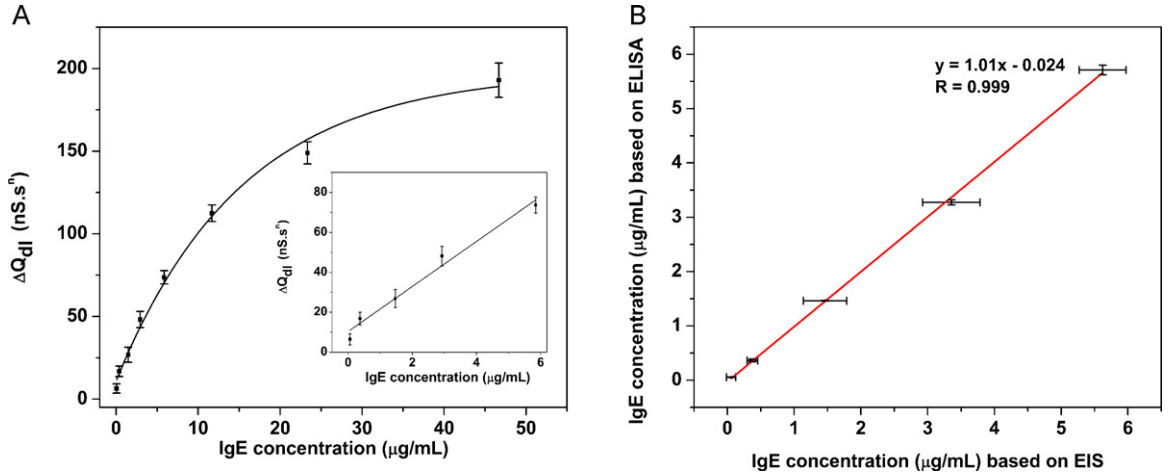

Fig. 5. (A) EIS responses of the diamond electrode to different IgE concentrations in human serum. Inset: the calibration curve of the aptasensor between the ΔQ_{dl} values and the IgE concentrations in the range of 0.05 mg/mL to 5.8 μg/mL. Each point represents the average of three measurements. Error bars present standard errors. (B) A correlation between the signals obtained by the ELISA kit and those obtained by the aptasensor for different IgE concentrations. The error bars represent the standard error of the mean based on three measurements of the same set of samples.

The aptasensor showed a linear trend between the ΔQ_{dl} values and the IgE concentrations up to 5.8 μg/mL with a coefficient of determination of 0.98 (inset of Fig. 5A). Above this concentration, the sensor reached saturation. Comparing to the data obtained in buffer, the aptasensor has a shorter linear dynamic range and less sensitivity. This might be due to the interference of the components in the serum. To validate the accuracy of the aptasensor, the IgE concentrations measured by EIS were plotted against those measured by the ELISA reference technique (Fig. 5B). An excellent correlation was found between the aptasensor and the ELISA for determination of IgE in serum samples with a correlation coefficient of 0.99. The slope of the correlation curve is 1.01 suggesting good clinical agreement between both techniques. It can be concluded that our aptasensor is definitely capable of quantifying IgE levels in serum. Although the detection limit of the ELISA kit (0.01 μg/mL) is somewhat lower than that of our system (0.03 μg/mL), the linear dynamic range of the EIS aptasensor is three times as broad as that of the ELISA benchmark. However, the standard error on the EIS measurements is still considerably large; work is in progress to reduce this variability. To further improve the sensor performance pre-treatment of the sensor surface, sample preparation and sensor miniaturization can be optimized.

4. Conclusions

We have demonstrated an impedimetric aptamer-based biosensor using NCD thin films as working electrodes for the label-free detection of human IgE. A linear relationship between capacitance and IgE concentration has been obtained throughout the concentration range of 0.03–42.8 μg/mL with a detection limit of 0.03 μg/mL. The NCD-based aptasensor developed in the present study is able to detect unlabeled human IgE. The aptasensor shows no change in electrical properties in the presence of IgG, thus exhibiting the minimal non-specific binding due to the application of BSA. It can also be reused for at least six cycles. We have illustrated that the EIS aptasensor works fine in real human serum samples. Although its linear dynamic range is three times as broad as that of the reference ELISA technique, further research is required to reduce the variability on the measurements.

Acknowledgments

The authors are grateful to the Flanders Fund for Research (FWO G.0603.08 and FWO G.0997.11), Interreg (project NanosensEU) and the Industrial Research Fund K.U. Leuven (IOF) (KP/06/011) for their financial support. V. Vermeeren (postdoctoral fellow), Jeroen Pollet (PhD student) and Lars grieten (PhD student) are funded by the 'Instituut voor aanmoediging van innovatie door Wetenschap en Technologie' (IWT).

References

Alfonta, L., Bardea, A., Khersonsky, O., Katz, E., Willner, I., 2001. Biosens. Bioelectron. 16, 675–687.
Berggren, C., Bjarnason, B., Johansson, G., 2001. Electroanalysis 13, 173–180.
Bijnens, N., Vermeeren, V., Daenen, M., Grieten, L., Haenen, K., Wenmackers, S., Williams, O.A., Ameloot, M., vandeVen, M., Michiels, L., Wagner, P., 2009. Phys. Status Solidi (a)-Appl. Math 206, 520–526.
Buravkova, L.B., Rykova, M.P., Gertsik, Y.G., Antropova, E.N., 2007. Acta Astronaut. 60, 254–258.
Cai, H., Xu, Y., He, P.G., Fang, Y.Z., 2003. Electroanalysis 15, 1864–1870.
Cooreman, P., Thoelen, R., Manca, J., vandeVen, M., Vermeeren, V., Michiels, L., Ameloot, A., Wagner, P., 2005. Biosens. Bioelectron. 20, 2151–2156.
German, I., Buchanan, D.D., Kennedy, R.T., 1998. Anal. Chem. 70, 4540–4545.
Gokulrangan, G., Unruh, J.R., Holub, D.F., Ingram, B., Johnson, C.K., Wilson, G.S., 2005. Anal. Chem. 77, 1963–1970.
Härtl, A., Schmich, E., Garrido, J.A., Hernando, J., Catharino, S.C.R., Walter, S., Feulner, P., Kromka, A., Steinmüller, D., Stutzmann, M., 2004. Nat. Mater. 3, 736–742.
Iijima, S., Shiba, K., Kurihara, Y., Kamei, S., Kimura, S., Kimura, M., Fukumura, Y., Kobayashi, I., 1999. J. Clin. Lab. Anal. 13, 145–150.
Jackola, D.R., Blumenthal, M.N., Rosenberg, A., 2004. Hum. Immunol. 65, 20–30.
Kara, P., Meric, B., Ozsoz, M., 2010. Comb. Chem. High Throughput Screen 13, 578–581.
Kharitonov, A.B., Alfonta, L., Katz, E., Willner, I., 2000. J. Electroanal. Chem. 487, 133–141.
Kim, Y.H., Kim, J.P., Han, S.J., Sim, S.J., 2009. Sens. Actuators B-Chem. 139, 471–475.
Koizumi, S., Kamo, M., Sato, Y., Ozaki, H., Inuzuka, T., 1997. Appl. Phys. Lett. 71, 1065–1067.
Lasseter, T.L., Cai, W., Hamers, R.J., 2004. Analyst 129, 3–8.
Lee, T.Y., Shim, Y.B., 2001. Anal. Chem. 73, 5629–5632.
Nebel, C.E., Shin, D.C., Rezek, B., Tokuda, N., Uetsuka, H., Watanabe, H., 2007. J. R. Soc. Interface 4, 439–461.
Pollet, J., Delport, F., Janssen, K.P.F., Jans, K., Maes, G., Pfeiffer, H., Wevers, M., Lammertyn, J., 2009. Biosens. Bioelectron. 25, 864–869.
Sampson, H.A., 1999. J. Allergy Clin. Immunol. 103, 717–728.
Smisdom, N., Smets, I., Williams, O.A., Daenen, M., Wenmackers, S., Haenen, K., Nesladek, M., D'Haen, J., Wagner, P., Rigo, J.M., Ameloot, M., vandeVen, M., 2009. Phys. Status Solidi A-Appl. Math. 206, 2042–2047.
Swain, G.M., Ramesham, R., 1993. Anal. Chem. 65, 345–351.
Tang, L., Tsai, C., Gerberich, W.W., Kruckeberg, L., Kania, D.R., 1995. Biomaterials 16, 483–488.
Uetsuka, H., Shin, D., Tokuda, N., Saeki, K., Nebel, C.E., 2007. Langmuir 23, 3466–3472.
Ushizawa, K., Sato, Y., Mitsumori, T., Machinami, T., Ueda, T., Ando, T., 2002. Chem. Phys. Lett. 351, 105–108.
Vermeeren, V., Bijnens, N., Wenmackers, S., Daenen, M., Haenen, K., Williams, O.A., Ameloot, M., Vandeven, A., Wagner, P., Michiels, L., 2007. Langmuir 23, 13193–13202.
Vermeeren, V., Wenmackers, S., Daenen, M., Haenen, K., Williams, O.A., Ameloot, M., vandeVen, M., Wagner, P., Michiels, L., 2008. Langmuir 24, 9125–9134.
Wei, F., Sun, B., Guo, Y., Zhao, X.S., 2003. Biosens. Bioelectron. 18, 1157–1163.
Wenmackers, S., Vermeeren, V., vandeVen, M., Ameloot, M., Bijnens, N., Haenen, K., Michiels, L., Wagner, P., 2009. Phys. Status Solidi A-Appl. Math. 206, 391–408.
Wiegand, T.W., Williams, P.B., Dreskin, S.C., Jouvin, M.H., Kinet, J.P., Tasset, D., 1996. J. Immunol. 157, 221–230.
Williams, O.A., Nesladek, M., 2006. Phys. Status Solidi A 203, 3375–3386.
Wuthrich, B., Schindler, C., Medici, T.C., Zellweger, J.P., Leuenberger, P., 1996. Int. Arch. Allergy Immunol. 111, 396–402.
Xu, D.K., Xu, D.W., Yu, X.B., Liu, Z.H., He, W., Ma, Z.Q., 2005. Anal. Chem. 77, 5107–5113.
Yang, W.S., Auciello, O., Butler, J.E., Cai, W., Carlisle, J.A., Gerbi, J., Gruen, D.M., Knickerbocker, T., Lasseter, T.L., Russell, J.N., Smith, L.M., Hamers, R.J., 2002. Nat. Mater. 1, 253–257.
Yang, W.S., Butler, J.E., Russell, J.N., Hamers, R.J., 2004. Langmuir 20, 6778–6787.
Yao, C.Y., Qi, Y.Z., Zhao, Y.H., Xiang, Y., Chen, Q.H., Fu, W.L., 2009. Biosens. Bioelectron. 24, 2499–2503.